A Probabilistic Seismic Hazard Analysis of Northeast India

Sandip Das,[a] Ishwer D. Gupta,[b] and Vinay K. Gupta[a]

Seismic hazard maps have been prepared for Northeast India based on the uniform hazard response spectra for absolute acceleration at stiff sites. An approach that is free from regionalizing the seismotectonic sources has been proposed for performing the hazard analysis. Also, a new attenuation model for pseudo-spectral velocity scaling has been developed by using 261 recorded accelerograms in Northeast India. In the present study, the entire area of Northeast India has been divided into 0.1° grid size, and the hazard level has been assessed for each node of this grid by considering the seismicity within a 300-km radius around the node. Using the past earthquake data, the seismicity for the area around each node has been evaluated by defining *a* and *b* values of the Gutenberg-Richter recurrence relationship, while accounting for the incompleteness of the earthquake catalogue. To consider the spatial distribution of seismicity around each node, a spatially smoothed probability distribution function of the observed epicentral distances has been used. Uniform hazard contours for pseudo-spectral acceleration as the hazard parameter have been obtained for an exposure time of 100 years and for 50% confidence level at different natural periods for both horizontal and vertical components of ground motion. The trends reflected by these contours are broadly consistent with the major seismotectonic features in the region.
[DOI: 10.1193/1.2163914]

INTRODUCTION

Seismic hazard analysis plays an important role in the earthquake-resistant design of structures by providing a rational value of input hazard parameters, like peak ground acceleration (PGA) or the response spectrum amplitudes at different natural periods. Traditionally, PGA has been a popular hazard parameter, but it is often found to be poorly correlated with the damage potential of ground motion. Hence it is increasingly being replaced by pseudo-spectral velocity (PSV) or pseudo-spectral acceleration (PSA), which are considered to be more comprehensive in describing the hazard levels. All the existing studies on seismic zoning of India have been made only in terms of the peak ground acceleration and by using the attenuation relations for some other parts of the world (Kaila and Rao 1979, Basu and Nigam 1978, Khattri et al. 1984, Bhatia et al. 1999). To utilize such studies for practical design applications, one needs to have a normalized spectral shape, which conceptually has several drawbacks (Trifunac 1992, Gupta 2002). To overcome these shortcomings, a probabilistic seismic hazard analysis

[a] Department of Civil Engineering, IIT Kanpur, Kanpur, UP 208016, India
[b] Central Water and Power Research Station, Khadakwasla, Pune, Maharashtra 411024, India

has been carried out in this study, and seismic hazard maps have been prepared for Northeast India[1] in terms of the PSA amplitudes at different natural periods.

The advantages of the probabilistic seismic hazard analysis (PSHA) approach are well known. The seismic hazard at a site is influenced by all the earthquakes with different magnitudes and distances, and PSHA is able to correctly reflect the actual knowledge of seismicity (Orozova and Suhadolc 1999). Along with the bigger events, smaller events are also important in hazard estimation, due to their higher occurrence rates (Wheeler and Mueller 2001). The essence of PSHA lies in the uniform hazard spectrum (UHS), which is a convenient tool to compare the hazard representations of different sites (Trifunac 1990, Todorovska et al. 1995, Peruzza et al. 2000). PSHA can be carried out in various ways depending on how one defines the model of seismicity.

To define the seismicity it is necessary to identify the various seismic sources in the area of a site, and this generally requires considerable personal judgment. Use of multiple scenarios is the latest development in the PSHA, wherein weights are assigned to each possibility and the final results are obtained as the weighted average (Wahlström and Grünthal 2001, Bernreuter et al. 1989, SSHAC 1997, EPRI 1986). To avoid the personal judgment and subjectivity, a regionalization-free approach has been proposed in the present study based only on the available earthquake catalog data for about the past 200 years without explicitly considering the hazard from known faults in the region. Other similar approaches have been proposed and used in the past by Veneziano et al. (1984), Frankel (1995), Woo (1996), and many others. As the available data show good correlation with all the known tectonic features in the Northeast India, the average trend of past seismicity can be considered to represent the future trend with good confidence. Therefore, earthquake recurrence relation is first defined by using all the past data within a 300-km radius of a site, with incompleteness of smaller magnitude earthquakes taken into account. The total average seismicity represented by this recurrence relation is then distributed with respect to distance by developing a smoothed probability distribution function of the epicentral distances of the past earthquakes from the site of interest. In addition to the seismicity, PSHA also requires an attenuation model specific to the region that could be used to estimate the ground motion with a specified confidence level for any magnitude and distance combination. In the present case, a spectral attenuation relationship is desirable since the target is to estimate the UHS at various sites of the region. For Northeast India, no such attenuation relationship is available to date. Hence an attenuation model based on PSV scaling is developed by using a total of 261 accelerograms from six different earthquake events.

To prepare the seismic hazard maps, the entire region of Northeast India is covered by considering about 2,500 equally spaced sites. Seismicity for each of these sites is determined by defining the Gutenberg-Richter (G-R) magnitude-frequency relationship (Gutenberg and Richter 1944) using past earthquake events within a 300-km radius of the site. For obtaining the UHS at a site, the probability that a given value of PSV at a

[1] Northeast India is the easternmost region of India, consisting of the following states: Nagaland, Arunachal Pradesh, Mizoram, Manipur, Meghalaya, Tripura, and Assam. The states border Myanmar, Tibet, Bangladesh, Nepal, and Bhutan, but only share a 50-km common border with the rest of India.

Table 1. Details of the earthquakes contributing the strong motion data

EQ #	Name of EQ	Date	Epicenter Lat (N)	Epicenter Long (E)	Earthquake Magnitude M_S	MMI Max.	Focal Depth h (km)	No. of Records
1	Meghalaya	10 Sep 86	25.564	92.220	5.5	VI	28	11
2	N.E. India	18 May 87	25.479	93.598	5.7	V	50	14
3	N.E. India	6 Feb 88	25.500	91.460	5.8	VII	15	17
4	Burma Border	6 Aug 88	25.384	94.529	7.2	VII	91	28
5	W. Burma	10 Jan 90	24.750	95.240	6.1	VII	119	10
6	W. Burma	6 May 95	25.010	95.340	6.4	VI	122	7

natural period will be exceeded is estimated by adopting the formulation of Anderson and Trifunac (1977) based on the Poissonian model of earthquake occurrences, though more generalized models are also available (Lee 1992, Todorovska 1994). With the hazard levels known at various sites in the form of several sets of UHS for different probabilities of exceedance, seismic hazard maps are obtained in terms of PSA contours for 50% confidence level and an exposure period of 100 years. These maps are expected to provide a more realistic distribution of seismic hazard at various wave periods than the use of a map in terms of PGA and a standard spectral shape. However, these may not be appropriate for the purpose of building code, where large areas are generally characterized by uniform hazard. Further, the proposed maps are only appropriate for relatively short return periods of ground motions and large probabilities of exceedance.

ATTENUATION MODEL FOR NORTHEAST INDIA

DATABASE USED

To develop a spectral attenuation model specific to Northeast India, a total of 261 accelerograms recorded from six earthquake events at different stations in the region have been used. Table 1 lists the details of the contributing earthquakes, which span a surface wave magnitude range of 5.5 to 7.2 (the epicenters of these events are also shown in Figure 8 as filled circles). These records are obtained from IIT Roorkee, and details of the data for the first four earthquakes are available in Chandrasekaran and Das (1993). The focal depths of these earthquakes vary over a wide range of 15 km to 122 km. In fact, Earthquakes #4, 5, and 6 are the subduction zone earthquakes, and only Earthquakes #1 and 3 are of crustal nature. Earthquake # 2 occurred in the interface zone.

The number of three-component records contributed by each earthquake over epicentral distances up to 300 km is also indicated in Table 1. There are a total of 87 such records providing a total of 261 acceleration components. The list of the recording stations is given in Table 2. This indicates that all the records have been obtained either on stiff sites or on soft sedimentary rocks. Figure 1 shows the histogram of the epicentral distances for all the records, with the number of the records on stiff soil sites indicated

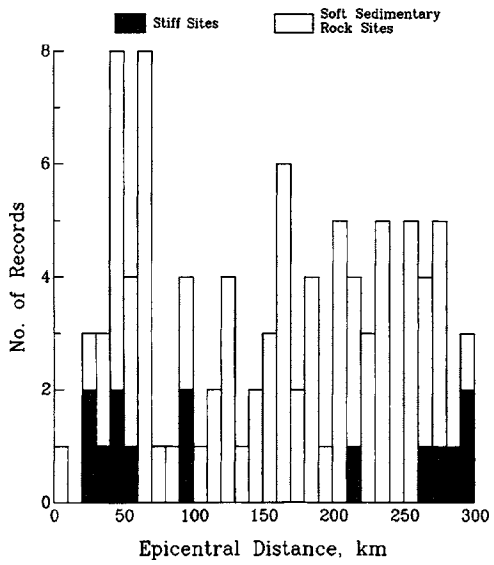

Figure 1. Histogram of the epicentral distances of records in the database.

by shaded heights. However, to develop the present attenuation relation, all the records are considered together to represent the stiff site condition. From the plot in Figure 1, it is also seen that there are a significant number of records in all the distance ranges, and that there is no gap in the data in any particular distance range. The minimum distance of recording is 8.7 km.

All the 261 accelerograms used in this study were obtained as 70-mm film records and were digitized using an automatic digitization hardware and software combination (Lee and Trifunac 1979). Those were then corrected for the dynamic response of the instrument and for the baseline distortions, by using the methodology attributable to Trifunac (1971, 1972). To apply the corrections, a variable frequency band was used for each accelerogram, for which the ground motion amplitudes were found to be higher than the noise level of the overall digitization process. Pseudo-spectral velocity (PSV) spectra have been computed for all the (corrected) accelerograms. As the horizontal ground motion at a site has strong azimuthal dependence, the PSV amplitudes for the two horizontal components at a station have been combined through square-root-of-sum-of-squares (SRSS) combination in order to normalize for this dependence. The so-obtained PSV spectrum needs to be divided by $\sqrt{2}$ to get the spectrum for a single horizontal component, which is slightly more conservative than the commonly used geometric mean. Thus a total of 87 horizontal spectra (obtained by SRSS combination) and 87 vertical spectra have been used for developing the attenuation model. The damping ratio considered for these computations is 5 percent of critical.

Table 2. List of recording stations

Station No.	Station Name	Site Condition	Location	
			Lat (N)	Long (E)
1	Baigao	Soft Rock	25.400	92.867
2	Baithalangso	Soft Rock	25.967	92.600
3	Bamungao	Soft Rock	25.900	93.017
4	Berlongfer	Soft Rock	25.767	93.250
5	Bokajan	Soft Rock	26.017	93.767
6	Cherrapunji	Firm Ground	25.267	91.733
7	Dauki	Soft Rock	25.200	92.033
8	Diphu	Soft Rock	25.917	93.433
9	Doloo	Soft Rock	24.917	92.783
10	Gunjung	Soft Rock	25.317	93.017
11	Haflong	Soft Rock	25.167	93.017
12	Hajadisa	Soft Rock	25.383	93.300
13	Harengajao	Soft Rock	25.117	92.867
14	Hatikhali	Soft Rock	25.650	93.117
15	Hojai	Soft Rock	26.000	92.850
16	Jellalpur	Soft Rock	25.000	92.467
17	Jhirighat	Soft Rock	24.800	93.117
18	Kalain	Soft Rock	24.983	92.583
19	Katakhal	Soft Rock	24.833	92.633
20	Khliehriat	Firm Ground	25.350	92.367
21	Koomber	Soft Rock	24.950	93.017
22	Laisong	Soft Rock	25.200	93.317
23	Maibang	Soft Rock	25.300	93.133
24	Mawphlang	Firm Ground	25.450	91.767
25	Nongkhlaw	Firm Ground	25.683	91.633
26	Nongpoh	Soft Rock	25.917	91.883
27	Nongstoin	Firm Ground	25.517	91.267
28	Panimur	Soft Rock	25.667	92.800
29	Pynursla	Firm Ground	25.300	91.917
30	Saitsama	Soft Rock	25.717	92.383
31	Shillong	Soft Rock	25.567	91.900
32	Silchar	Soft Rock	24.833	92.800
33	Ummulong	Soft Rock	25.517	92.167
34	Umrongso	Soft Rock	25.517	92.633
35	Umsning	Soft Rock	25.733	91.883

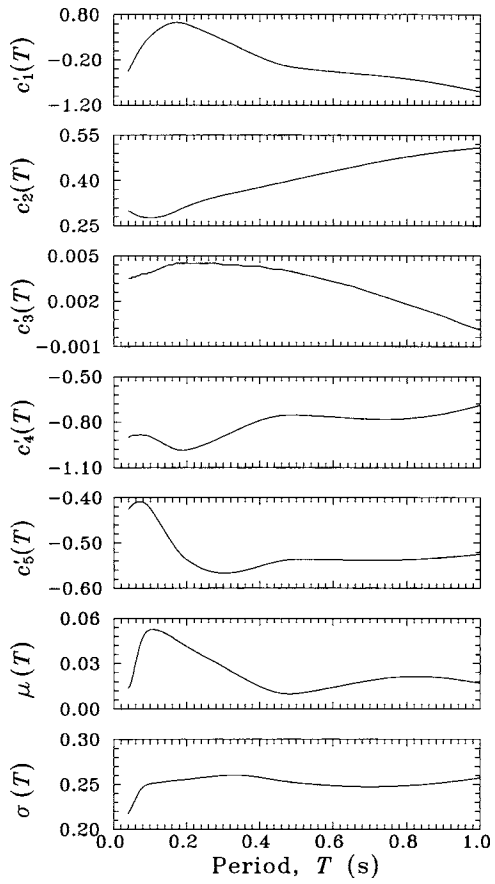

Figure 2. Variation of estimated (smoothed) regression coefficients with T.

ATTENUATION RELATION

Prior to performing regression analysis on the PSV data, it is necessary to select a functional form of attenuation model in terms of the parameters that govern the attenuation of ground shaking. In spite of apparent differences in the functional forms, an examination of the various published attenuation relations (Douglas 2001, 2002) indicates that all of them include terms for geometrical spreading and magnitude scaling, with some considering the anelastic attenuation effects also. Trifunac and coworkers (1980, 1989) have proposed a functional form by using a frequency-dependent attenuation function in terms of a representative source-to-site distance (Trifunac and Lee 1990), and by taking care of both horizontal and vertical motions simultaneously. The site soil and geological conditions in different published relations are defined and treated in a wide variety of ways. As only a limited database is available and a detailed description of the input parameters is lacking in the present situation, the following simplified form has been used to describe the attenuation characteristics in the present study:

$$\log[\mathrm{PSV}(T)] = c_1(T) + c_2(T)M + c_3(T)h + c_4(T)\log(\sqrt{R^2 + h^2}) + c_5(T)v \qquad (1)$$

where M is the earthquake magnitude, R is the epicentral distance, h is the focal depth, and v is an index variable taken as zero for horizontal motion and 1 for vertical motion. In Equation 1, the term $c_3(T)h$ has been added to take care of the wide range of the focal depths (15 km to 122 km) of the contributing earthquakes as given in Table 1. The deeper earthquakes are in general recorded at very long distances, and hence the logarithm of hypocentral distance alone is unable to account for the dependence on h. The direct linear term $c_3(T)h$ is therefore included to account for the dependence on the focal depth. The spectral amplitude PSV(T) at natural period, T, of a single-degree-of-freedom oscillator is defined in the units of m/s. Further, $c_1(T)$, $c_2(T)$, $c_3(T)$, $c_4(T)$, and $c_5(T)$ are the coefficients to be evaluated by the regression analysis on the available PSV data. A single relation for both horizontal and vertical motions is used because the distance attenuation and the magnitude scaling for the elastic waves generating these motions cannot be differentiated on physical grounds. Further, this helps to increase the number of data points and thus to provide more stable estimates of the regression coefficients.

In order to obtain unbiased estimates of regression coefficients in Equation 1, the regression analysis is performed in two stages as in Joyner and Boore (1981). In the first stage, the first three terms involving coefficients, $c_1(T)$, $c_2(T)$, and $c_3(T)$, are combined to give event-dependent terms, $a_1(T), a_2(T), \ldots, a_n(T)$, for n total number of events. These terms and the coefficients $c_4(T)$ and $c_5(T)$ are estimated by performing linear regression analysis on the following model:

$$\log[\mathrm{PSV}(T)] = \sum_{i=1}^{n} a_i(T)e_i + c_4(T)\log(\sqrt{R^2 + h^2}) + c_5(T)v \qquad (2)$$

Here, e_i denotes 1 for the ith earthquake event and zero otherwise. Through this step, the coefficients $c_4(T)$ and $c_5(T)$ are decoupled from the other three coefficients. The remaining coefficients, $c_1(T)$, $c_2(T)$, and $c_3(T)$, are now determined by performing the linear regression analysis on the equation

$$a(T) = c_1(T) + c_2(T)M + c_3(T)h \qquad (3)$$

where $a(T)$ takes n (=6) values, $a_1(T), a_2(T), \ldots, a_n(T)$, as determined from Equation 2.

The regression analysis is performed only for periods up to 1.0 s, as for the longer periods, PSV amplitudes for the accelerograms are found to be below the noise level. Figure 2 shows the estimated (smoothed) values of the regression coefficients, i.e., $c_1'(T)$, $c_2'(T)$, $c_3'(T)$, $c_4'(T)$, and $c_5'(T)$. In Table 3, these values are listed at 51 natural periods between 0.04 and 1.0 s. It is observed from Figure 2 that the value of $c_3'(T)$, which reflects the possible effects of focal depth for a fixed hypocentral distance, is positive and significant at higher frequencies, and becomes insignificant at longer periods. This is expected since the deeper earthquakes are supposed to produce more high-

Table 3. Estimated (smoothed) values of the regression coefficients

Period, T	$c_1'(T)$	$c_2'(T)$	$c_3'(T)$	$c_4'(T)$	$c_5'(T)$	$\mu(T)$	$\sigma(T)$
0.040	−0.4405	0.2993	0.0035	−0.9007	−0.4252	0.0140	0.2179
0.042	−0.4114	0.2981	0.0035	−0.8974	−0.4231	0.0145	0.2192
0.044	−0.3815	0.2969	0.0035	−0.8945	−0.4211	0.0154	0.2205
0.046	−0.3507	0.2955	0.0035	−0.8921	−0.4192	0.0166	0.2220
0.048	−0.3192	0.2942	0.0035	−0.8904	−0.4175	0.0183	0.2237
0.050	−0.2872	0.2928	0.0036	−0.8892	−0.4160	0.0203	0.2254
0.055	−0.2075	0.2895	0.0036	−0.8876	−0.4131	0.0258	0.2300
0.060	−0.1297	0.2864	0.0036	−0.8865	−0.4108	0.0313	0.2344
0.065	−0.0552	0.2837	0.0037	−0.8858	−0.4091	0.0364	0.2384
0.070	0.0148	0.2813	0.0037	−0.8855	−0.4084	0.0409	0.2420
0.075	0.0794	0.2794	0.0038	−0.8855	−0.4085	0.0447	0.2449
0.080	0.1386	0.2779	0.0038	−0.8859	−0.4097	0.0477	0.2471
0.085	0.1924	0.2768	0.0038	−0.8870	−0.4119	0.0499	0.2487
0.090	0.2413	0.2761	0.0038	−0.8890	−0.4152	0.0514	0.2498
0.095	0.2854	0.2757	0.0039	−0.8922	−0.4195	0.0522	0.2505
0.100	0.3249	0.2757	0.0039	−0.8969	−0.4247	0.0526	0.2510
0.110	0.3962	0.2765	0.0040	−0.9084	−0.4364	0.0525	0.2515
0.120	0.4609	0.2780	0.0041	−0.9211	−0.4489	0.0521	0.2520
0.130	0.5171	0.2804	0.0042	−0.9346	−0.4618	0.0513	0.2525
0.140	0.5631	0.2837	0.0043	−0.9482	−0.4749	0.0502	0.2530
0.150	0.5973	0.2879	0.0044	−0.9610	−0.4879	0.0489	0.2535
0.160	0.6190	0.2928	0.0044	−0.9720	−0.5004	0.0474	0.2540
0.170	0.6281	0.2983	0.0045	−0.9803	−0.5119	0.0458	0.2544
0.180	0.6252	0.3039	0.0045	−0.9854	−0.5222	0.0442	0.2548
0.190	0.6114	0.3094	0.0045	−0.9865	−0.5309	0.0427	0.2552
0.200	0.5879	0.3144	0.0045	−0.9837	−0.5376	0.0412	0.2556
0.220	0.5282	0.3235	0.0045	−0.9718	−0.5480	0.0384	0.2565
0.240	0.4623	0.3317	0.0045	−0.9563	−0.5562	0.0358	0.2574
0.260	0.3917	0.3390	0.0045	−0.9378	−0.5619	0.0331	0.2584
0.280	0.3180	0.3454	0.0045	−0.9169	−0.5654	0.0305	0.2593
0.300	0.2420	0.3512	0.0044	−0.8947	−0.5667	0.0278	0.2600
0.320	0.1647	0.3566	0.0044	−0.8719	−0.5661	0.0251	0.2603
0.340	0.0869	0.3617	0.0044	−0.8493	−0.5639	0.0224	0.2603
0.360	0.0097	0.3667	0.0043	−0.8279	−0.5605	0.0197	0.2598
0.380	−0.0657	0.3719	0.0043	−0.8082	−0.5563	0.0172	0.2589
0.400	−0.1376	0.3772	0.0043	−0.7909	−0.5517	0.0148	0.2578
0.420	−0.2040	0.3826	0.0042	−0.7766	−0.5471	0.0128	0.2564
0.440	−0.2626	0.3880	0.0041	−0.7656	−0.5430	0.0112	0.2550
0.460	−0.3114	0.3935	0.0041	−0.7582	−0.5397	0.0102	0.2537
0.480	−0.3490	0.3988	0.0040	−0.7545	−0.5376	0.0098	0.2526
0.500	−0.3751	0.4042	0.0039	−0.7545	−0.5368	0.0101	0.2517
0.550	−0.4217	0.4174	0.0036	−0.7603	−0.5368	0.0119	0.2500
0.600	−0.4611	0.4307	0.0033	−0.7679	−0.5375	0.0142	0.2486

Table 3. (**cont.**)

Period, T	$c_1'(T)$	$c_2'(T)$	$c_3'(T)$	$c_4'(T)$	$c_5'(T)$	$\mu(T)$	$\sigma(T)$
0.650	−0.4972	0.4438	0.0030	−0.7758	−0.5384	0.0166	0.2477
0.700	−0.5335	0.4566	0.0026	−0.7817	−0.5388	0.0187	0.2474
0.750	−0.5733	0.4684	0.0022	−0.7834	−0.5385	0.0204	0.2477
0.800	−0.6200	0.4789	0.0018	−0.7787	−0.5374	0.0213	0.2486
0.850	−0.6762	0.4881	0.0014	−0.7663	−0.5353	0.0213	0.2501
0.900	−0.7431	0.4960	0.0010	−0.7462	−0.5324	0.0205	0.2522
0.950	−0.8196	0.5030	0.0005	−0.7199	−0.5289	0.0189	0.2546
1.000	−0.9018	0.5096	0.0001	−0.6900	−0.5251	0.0170	0.2573

frequency body-wave motions than the shallower earthquakes of the same magnitude and hypocentral distance, due to less anelastic attenuation and greater stress drop (McGarr 1984).

By using the estimated regression coefficients, the estimated value of $\log[\mathrm{PSV}(T)]$ becomes

$$\log[\mathrm{PSV}'(T)] = c_1'(T) + c_2'(T)M + c_3'(T)h + c_4'(T)\log(\sqrt{R^2+h^2}) + c_5'(T)v \tag{4}$$

With $\mathrm{PSV}(T)$ representing the actual values of PSV spectra for an accelerogram, the residuals $\epsilon(T)$ for all 174 PSV spectra are calculated as

$$\epsilon(T) = \log[\mathrm{PSV}(T)] - \log[\mathrm{PSV}'(T)] \tag{5}$$

The observed probability distribution of the residuals, i.e., $p^*(\epsilon(T))$, at each period T can be obtained from the percentiles of the observations below different amplitudes of $\epsilon(T)$ as computed from Equation 5. However, assuming that the residuals follow a normal distribution with the mean, $\mu(T)$, and standard deviation, $\sigma(T)$, the theoretical probability distribution can be defined as

$$p(\epsilon(T)) = \frac{1}{\sigma(T)\sqrt{2\pi}} \int_{-\infty}^{\epsilon(T)} e^{-\frac{1}{2}\left(\frac{x-\mu(T)}{\sigma(T)}\right)^2} \mathrm{d}x \tag{6}$$

The maximum likelihood estimators of $\mu(T)$ and $\sigma(T)$ are calculated from $p^*(\epsilon(T))$ (by calculating the mean and standard deviation of residuals at time period T), and then are smoothed along T. These smoothed values, say $\hat{\mu}(T)$ and $\hat{\sigma}(T)$, are also shown in Figure 2 and listed in Table 3, which may be used to estimate $\epsilon(T)$ at a given period T (by using Equation 6) corresponding to a specified level of confidence, p. Figure 3 shows the comparison of these estimated residuals with the actual residuals, for $p(\epsilon, T)$ and $p^*(\epsilon, T) = 0.1$ (10%) to 0.9 (90%). The zig-zag solid lines in the figure represent the actual residuals, while the smooth dashed lines represent the estimated residuals. The reliability of the assumption that residuals are normally distributed, has been checked by two well-known statistical "goodness-of-fit" tests, namely the chi-square and Kolmogorov-Smirnov (KS) tests. Both tests have been conducted at 51 periods, and chi-

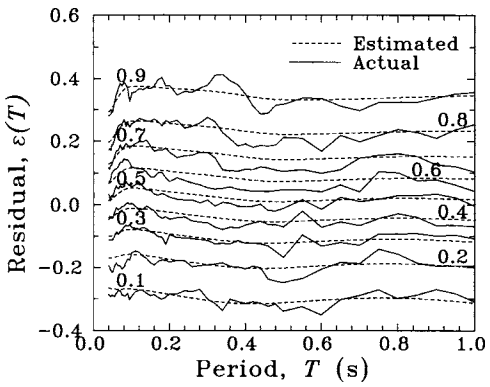

Figure 3. Residual spectra for nine different values of $p(\epsilon, T)$ between 0.1 and 0.9 at intervals of 0.1.

square statistics, $\chi^2(T)$, and KS statistics, KS(T), have been found to be well within their 95% cut-off values at all the natural periods. Using the estimated residuals, $\epsilon(p, T)$, and adding those to the least-square estimate as in Equation 4, the PSV spectrum for a desired level of confidence, p, may be obtained as

$$\log[\mathrm{PSV}'(p,T)] = c_1'(T) + c_2'(T)M + c_3'(T)h + c_4'(T)\log(\sqrt{R^2+h^2}) + c_5'(T)v + \epsilon(p,T) \tag{7}$$

ILLUSTRATION OF THE PROPOSED MODEL

Figures 4 and 5 show typical comparison of the PSV spectra computed from the recorded accelerograms, for a small and shallow event (18 May 1987) with M=5.7, h =50 km, with the PSV spectra estimated (by using Equation 7) for confidence levels of 0.1 and 0.9. Figure 4 shows the comparison for the horizontal spectrum recorded at the Hatikhali station with R=53.51 km, while Figure 5 shows the comparison for the vertical spectrum recorded at the Berlongfer station with R=47.41 km. In these figures, the pair of top (p=0.9) and bottom (p=0.1) PSV curves (in solid lines) outlines the 80% confidence interval of the predicted amplitudes, while the dashed line shows the actual spectrum. Figures 6 and 7 show similar comparison for a large and deep event (6 August 1988) with M=7.2, h=91 km. Figure 6 shows the comparison for the horizontal spectrum recorded at the Hajadisa station with R=123.50 km, while Figure 7 shows the comparison for the vertical spectrum recorded at the Gunjung station with R =153.91 km.

It is clear from the above four figures that the proposed model works well for both shallow and deep, and small and large events. It also works well for both near-source and distant sites. However, the 80% confidence band is wide enough to reflect a considerable

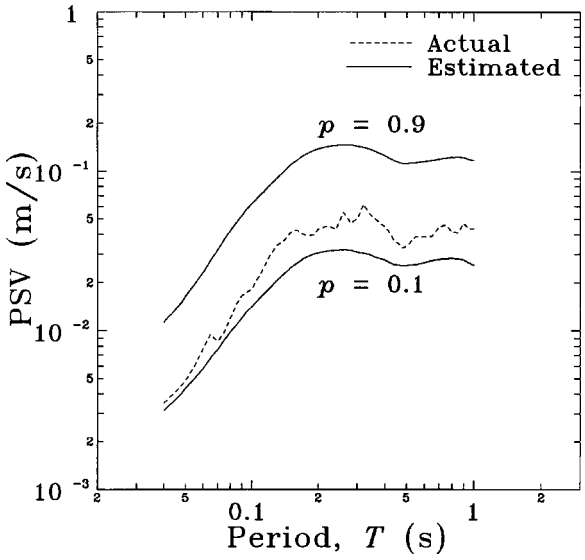

Figure 4. Comparison of actual and estimated horizontal PSV spectra for the Hatikhali record at 53.51 km due to the 18 May 1987 earthquake of magnitude 5.7 and focal depth 50 km.

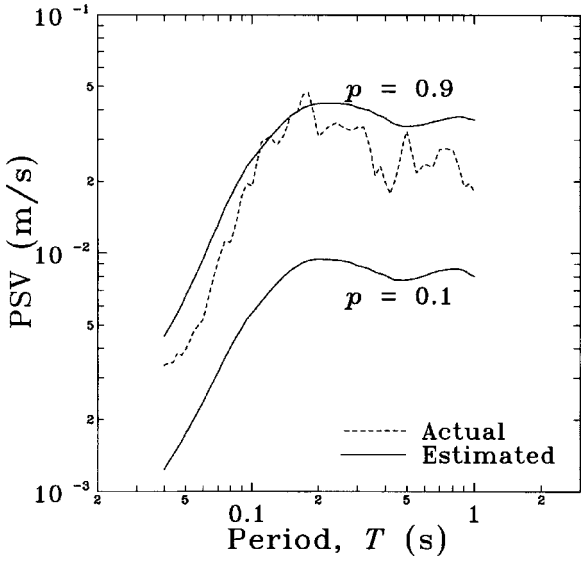

Figure 5. Comparison of actual and estimated vertical PSV spectra for the Berlongfer record at 47.41 km due to the 18 May 1987 earthquake of magnitude 5.7 and focal depth 50 km.

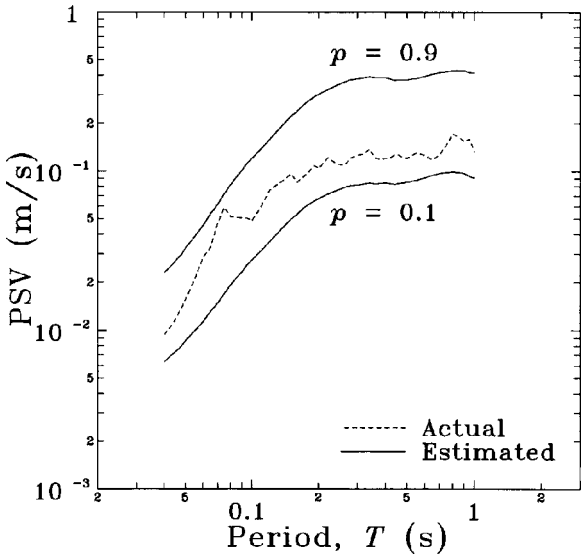

Figure 6. Comparison of actual and estimated horizontal PSV spectra for the Hajadisa record at 123.50 km due to the 6 August 1988 earthquake of magnitude 7.2 and focal depth 91 km.

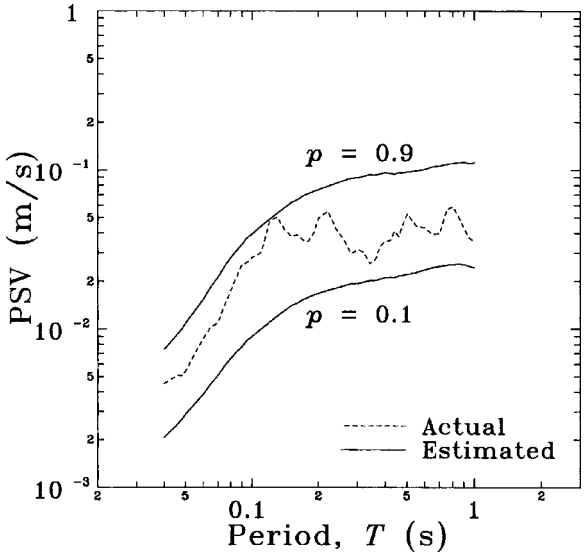

Figure 7. Comparison of actual and estimated vertical PSV spectra for the Gunjung record at 153.91 km due to the 6 August 1988 earthquake of magnitude 7.2 and focal depth 91 km.

amount of scatter, which is typical of strong motion data (Lee 2002). This highlights the level of uncertainty that comes from the attenuation model alone in a probabilistic seismic hazard analysis.

PROBABILISTIC SEISMIC HAZARD FORMULATION

The probabilistic seismic hazard analysis is based on evaluating the probability distribution function for the amplitudes, z, of a random parameter, Z, representing the strong ground motion at a site due to all the earthquakes expected to occur during a specified exposure period in the region around the site. Under the Poissonian assumption, this probability distribution is defined in terms of the annual rate, $\nu(z)$, of exceeding the ground motion level z at the site under consideration, due to all possible pairs, (M,R), of the magnitude and epicentral distance of the earthquake event expected around the site, with its random nature taken into account. To estimate the chance of exceeding level z due to magnitude M at distance R, it is necessary to have an attenuation relation for the ground motion parameter Z, which in the present study has been taken as the pseudo-spectral velocity, PSV(T), at a given natural period, T.

Cornell (1968) was probably the first to present a formulation for probabilistic seismic hazard analysis. However, he proposed the use of only the median attenuation relation to find $\nu(z)$ as the sum total of the annual occurrence rates for all (M,R) combinations, which produced the median ground motion level exceeding z. Thus the large random scattering of the recorded data that is normally present around the median attenuation was not accounted for in his formulation. Anderson and Trifunac (1978, 1977) incorporated the random uncertainties in the attenuation relations and defined the annual rate $\nu(z)$ as

$$\nu(z) = \sum_{i=1}^{I} \sum_{j=1}^{J} q(z|M_j,R_i)n(M_j,R_i) \tag{8}$$

Here, $q(z|M_j,R_i)$ is the probability of exceeding the ground motion level z due to an event of size M_j at distance R_i. The quantity $n(M_j,R_i)$ is the annual rate of occurrence of the (M_j,R_i) events. As the magnitude and distance are both continuous variables, for practical applications, those are discretized into small intervals $(M_j-\delta M_j/2, M_j+\delta M_j/2)$ and $(R_i-\delta R_i/2, R_i+\delta R_i/2)$ with central values, M_j and R_i. The summations over i and j in Equation 8 are thus taken over the total number of distance intervals, I, and the magnitude intervals, J, respectively. Assuming that $\nu(z)$ is the average occurrence rate of a Poisson process, the probability of exceeding z during an exposure period of Y years can be written as

$$P(Z > z) = 1 - \exp\{-Y\nu(z)\} \tag{9}$$

The plot of z versus $P(Z>z)$ is commonly termed as the hazard function.

The basic formulation constituted by the expressions of Equations 8 and 9 forms the core of the state-of-the-art PSHA employing logic tree formulation to account for the modeling uncertainties. In the logic tree approach, one accounts for such uncertainties,

due to lack of data and incomplete understanding of the exact physical process, by considering multiple scenarios with weights for the seismic source models, their expected seismicity, and the ground motion attenuation relations. The basic PSHA as described above is then performed, for all possible sets of the input parameters, to obtain multiple estimates of $\nu(z)$ with weights. These are used to get the expected (mean) value of $\nu(z)$, which is then used in Equation 9 to define the hazard function. In the present study, however, a more objective regionalization-free approach has been proposed to define the seismicity rates $n(M_j, R_i)$, as described in the next section. Also, only one model, as developed in the previous section by using strong-motion data specific to Northeast India, has been used to estimate the probability $q(z|M_j, R_i)$ for the PSV(T) amplitudes.

By using the PSHA formulation, the spectral amplitudes PSV(T) can be evaluated at all the natural periods for a constant probability of exceedance at a site. Such a response spectrum is commonly known as the uniform hazard spectrum (UHS). In addition to PSV, the functional can be any other property of ground motion, say, Fourier spectrum amplitude, power spectral density function, strong-motion duration, etc. In the present study, the functional is considered to be PSA due to this being a popular design parameter. For this, UHS is first obtained for the PSV functional (using the attenuation relationship developed for PSV), and then this is converted to the UHS for the PSA functional by multiplying with $2\pi/T$.

SEISMICITY OF NORTHEAST INDIA

For seismic hazard analysis, the entire region of Northeast India lying between 21°–30° latitude and 88°–97° longitude is considered. This is subdivided into a 0.1° latitude and 0.1° longitude grid, and the UHS are estimated for all the sites defined by the intersection points of the grid. For this purpose, the seismicity, $n(M_j, R_i)$, for each site is evaluated by fitting the G-R recurrence relation to the past earthquake data within a 300-km radius of the site, without identifying the seismotectonic source zones. The earthquake catalogue used covers the period from 1458 to 2000, where the data up to 1979 is taken from Bapat et al. (1983), and from the USGS web site for the subsequent period. The data corresponds to the geographical area between 18°–33° latitude and 85°–100° longitude. Figure 8 shows the correlation of the significant earthquakes, with magnitude above 5.0, with the major tectonic features in Northeast India (Verma et al. 1976). It is seen that although the epicenters are dispersed widely, they definitely follow the trends of the tectonic features. Thus the identification of the seismic source zones is expected to vary only slightly around the most likely trend defined by the epicentral distribution. Also, the available database is quite comprehensive with a total of about 3,000 events in the region of Figure 8. This can be used to estimate the expected occurrence rate of earthquakes in each magnitude range M_j, and to define in an objective way their spatial distribution with respect to each site, as discussed in the following.

According to the G-R relationship, the annual occurrence rate, $N(M)$, of earthquakes with magnitudes greater than or equal to M can be described by (Gutenberg and Richter 1944):

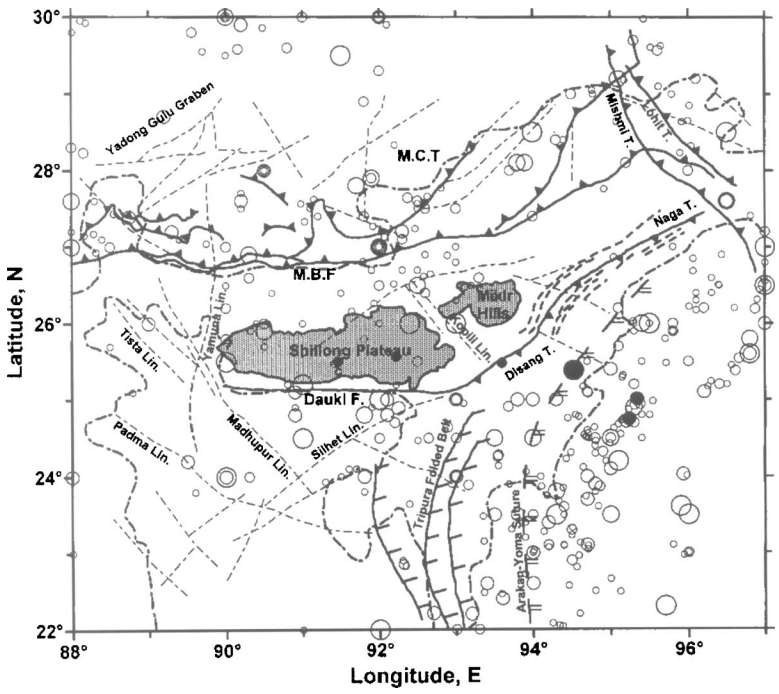

Figure 8. Correlation of the epicenters of past earthquakes with the major tectonic features in the Northeast India region.

$$\log N(M) = a - bM \tag{10}$$

where a and b are constants. Prior to estimating these constants, it is of crucial importance to check the completeness of earthquake data corresponding to different ranges of magnitude, particularly since the evaluation of seismicity here is entirely based on the past earthquake data. It is obvious that smaller earthquake events occur more frequently than the bigger ones, and hence the recurrence rates of smaller earthquakes can be evaluated even from the most recent data of the last 15–20 years. On the other hand, for bigger events one may have to consider a much longer time frame, say, that of about 100 years. Thus it is essential to identify the intervals of complete recording for different magnitude ranges, without which the recurrence rate may be underestimated for smaller events and overestimated for larger events.

To minimize the effects of incompleteness, an empirical and statistically simple method based on the stability of the magnitude recurrence rate is adopted here (Stepp 1973). According to this method, the entire catalogue of earthquake events is grouped into several magnitude ranges, and the average number of events per year, $R(M)$, are evaluated for each magnitude range for different time windows of increasing lengths, backward from the year of the most recent data. The so-obtained series of $R(M)$ is analyzed to give the smallest length of the time window for which $R(M)$ becomes station-

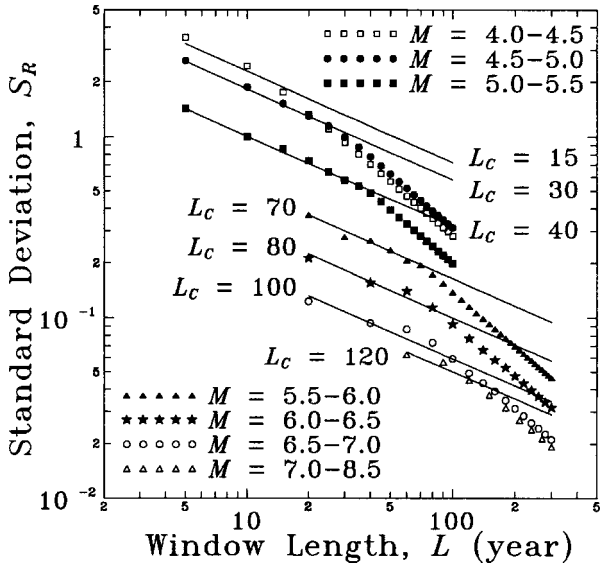

Figure 9. Completeness plots for different magnitude ranges in the entire area of Northeast India.

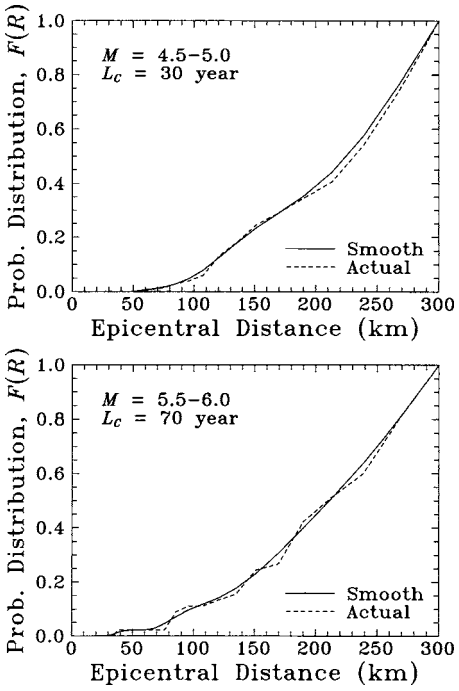

Figure 10. Typical examples of the observed and the smoothed distribution functions for the epicentral distances from a site in Northeast India.

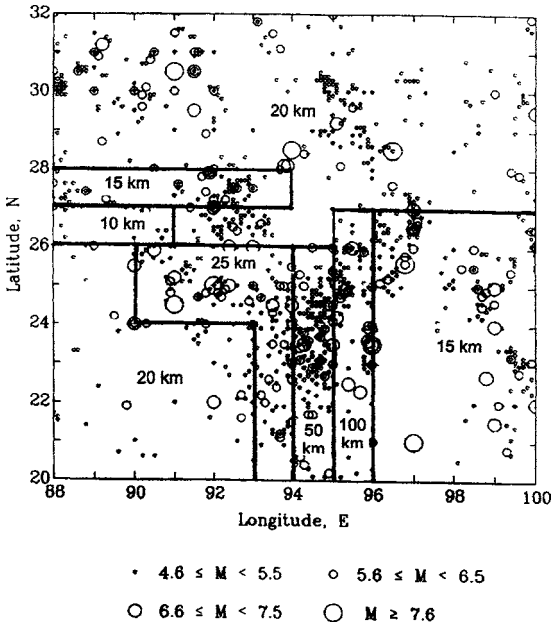

Figure 11. Idealized subregions of uniform average focal depths.

ary, and this window is assumed to represent the minimum period in which the complete reporting has taken place. $R(M)$ is modeled as a Poisson point process in time (Stepp 1973), such that for a window length of L years, the standard deviation of $R(M)$ is given by

$$S_R = \sqrt{\frac{R(M)}{L}} \tag{11}$$

Equation 11 implies that for stationary $R(M)$, S_R is supposed to vary as $\sqrt{1/L}$ with L. The plot of S_R as a function of L, known as the "completeness plot," shows such behavior until certain window length, and this length is taken as the period of completeness, L_C, for that magnitude range. The completeness periods for the complete Northeast India data are thus estimated to be 15, 30, 40, 70, 80, 100, and 120 years for the magnitude ranges of 4.0–4.5, 4.5–5.0, 5.0–5.5, 5.5–6.0, 6.0–6.5, 6.5–7.0, and 7.0–8.5, respectively, as shown in Figure 9.

To determine the a and b values (in Equation 10) for the area within a 300-km radius of each of the grid points, all past events (in the respective periods of completeness) with epicenters within the area are considered, and the annual rate, $N(M)$, is determined for different values of magnitude from $M_{\min}=4.0$ to $M_{\max}=8.5$. Fitting a least-squares straight line to the data points leads to the values of a and b, which are used to obtain the number of earthquakes, $\mathcal{N}(M_j)$, with magnitudes between $M_j - \delta M_j/2$ and $M_j + \delta M_j/2$ as

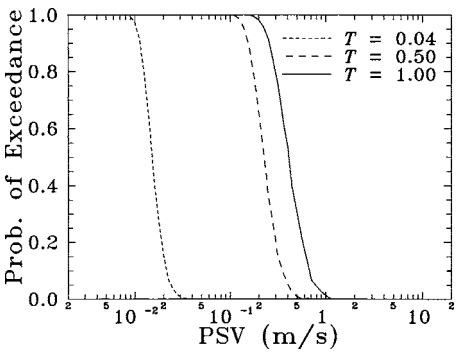

Figure 12. Typical hazard curves for PSV amplitudes at different natural periods.

$$\mathcal{N}(M_j) = N\left(M_j - \frac{\delta M_j}{2}\right) - N\left(M_j + \frac{\delta M_j}{2}\right) \tag{12}$$

It may be mentioned here that a maximum likelihood procedure (e.g., see Weichert 1980) would have been better (in place of the least-squares method) to estimate the values of a and b. However, since the Gutenberg-Richter's relation has been defined for the cumulative number of earthquakes (which provides a normalizing effect for the residual outliers), care has been taken for the incompleteness in the smaller magnitudes, and since a very small discretization interval of 0.1 has been used for the magnitude, the limitations of the least-squares method may not be of much consequence to the accuracy of the estimates obtained here. Weichert (1980) has also indicated that for well-constrained data, the least-squares method may lead to the results equivalent to the maximum likelihood estimates.

To complete the description of seismicity, it is necessary to spatially distribute the numbers $\mathcal{N}(M_j)$, as obtained from Equation 12, with respect to the site. For this purpose,

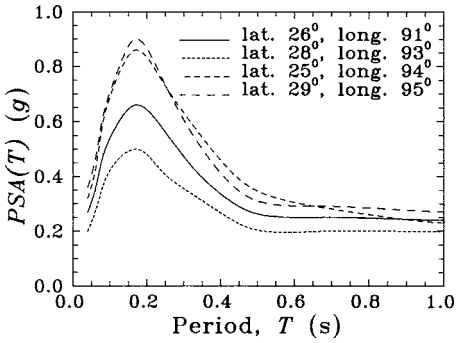

Figure 13. Uniform hazard PSA spectra (horizontal) for four different sites in Northeast India.

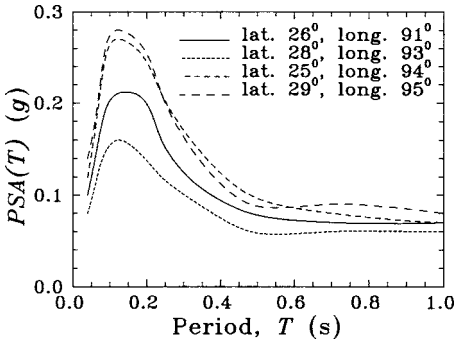

Figure 14. Uniform hazard PSA spectra (vertical) for four different sites in Northeast India.

the epicentral distances from the site for all the events in a selected magnitude range, which occurred during the estimated period of completeness, are first used to define the observed probability distribution function of the epicentral distance. To take care of the

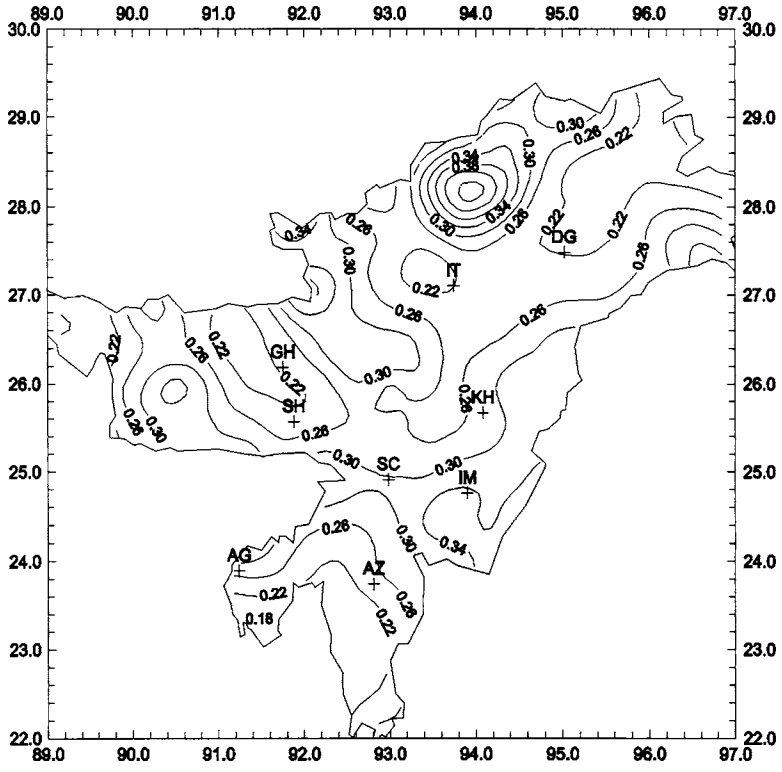

Figure 15. Hazard map for horizontal PSA (in g) at T=0.04 s.

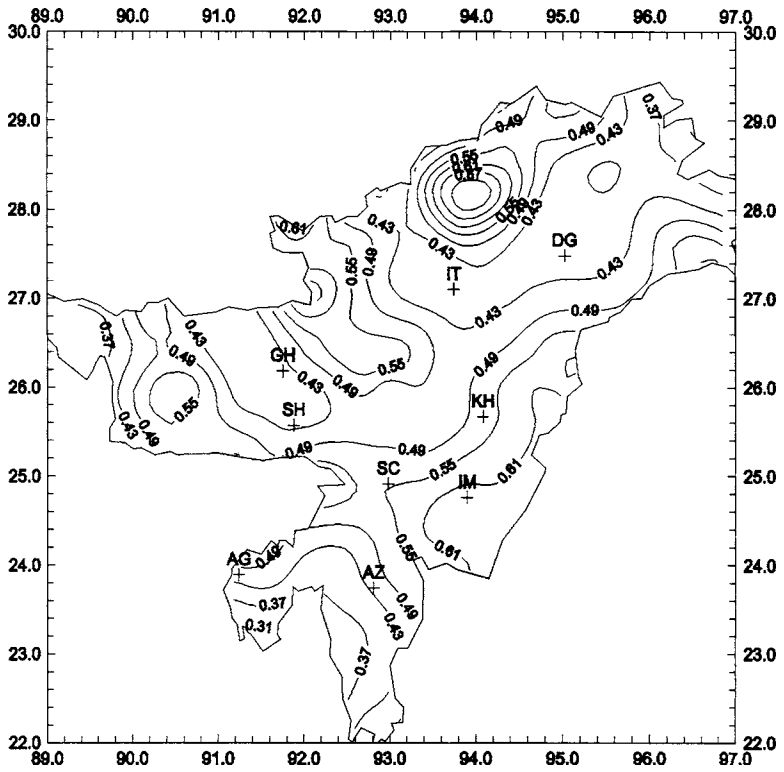

Figure 16. Hazard map for horizontal PSA (in g) at T=0.08 s.

fact that reported epicentral locations may be in some error and that some of the future events may also occur at the other nearby distances, this probability distribution function is smoothed by a running distance average. Typical examples of the unsmoothed and smoothed distribution functions are shown in Figure 10 for the magnitude ranges 4.5–5.0 and 5.5–6.0 in case of the (27.2° latitude, 93.7° longitude) grid point. The smoothed distribution function $F(R)$ for a particular magnitude range can be used to obtain the proportion of the total number of events in a given range of epicentral distance from the site under consideration. Thus the expected rate of events in a distance range $(R_i - \delta R_i/2, R_i + \delta R_i/2)$ can be obtained as

$$n(M_j, R_i) = \mathcal{N}(M_j)[F(R_i + \delta R_i/2) - F(R_i - \delta R_i/2)] \tag{13}$$

For the computation of the results in the present study, earthquake magnitude is discretized into nine intervals with central magnitudes M_j=4.25, 4.75, 5.25, ..., 8.25 and δM_j=0.5 for all the intervals. Further, it is assumed that the 300-km-radius area around the site is subdivided into 50 annular elements, equispaced on logarithmic scale, with each element acting as a source element at an epicentral distance R_i (R_i is the radius of the middle circle of the annular ring). The present formulation is thus based on the as-

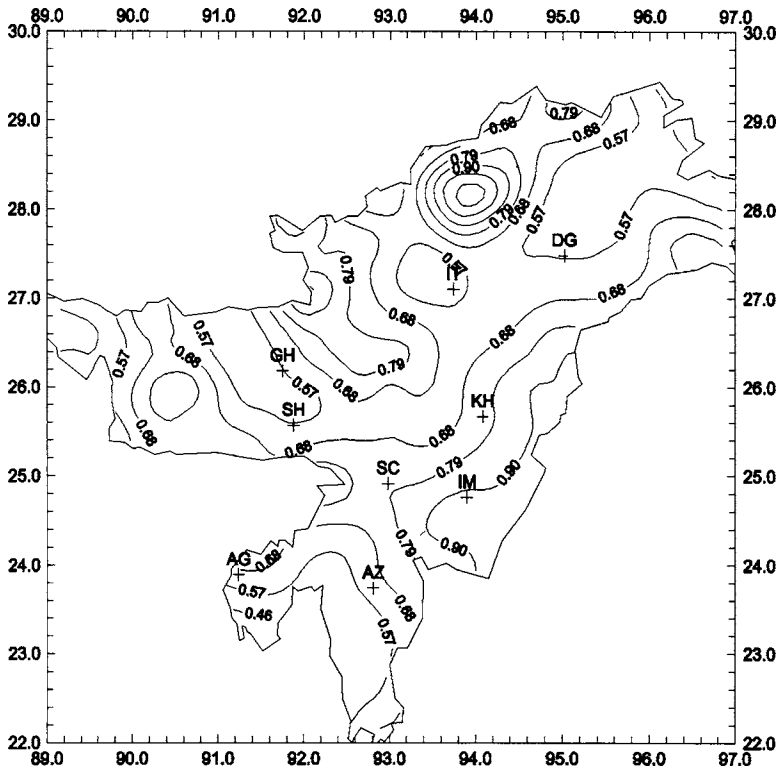

Figure 17. Hazard map for horizontal PSA (in g) at T=0.17 s.

sumption of a point source. As explained in the next section, each combination of M_j and R_i is also assigned a suitable focal depth to compute the probability of exceedance for different values of spectral amplitudes. A consistent application of the parameters in the attenuation relation developed and used in the present study is thus expected to provide quite realistic estimate of UHS. However, if the earthquake source is considered to have a finite rupture length and the distance R_i for each M_j is taken to be the closest distance from the fault rupture, the results may be too conservative (Anderson and Trifunac 1977, 1978).

UNIFORM HAZARD MAPS FOR NORTHEAST INDIA

From the knowledge of $n(M_j,R_i)$ for a site in Northeast India, and for a given exposure period, the probability distribution of Equation 9 can be computed for the PSV spectrum at any specified natural period, T, by evaluating the probability, $q(PSV(T)|M_j,R_i)$, from the attenuation relation developed (see Equation 7). For the computation of $q(PSV(T)|M_j,R_i)$, it is also necessary to assign the focal depth to each combination of M_j and R_i for the seismicity around the site. For this purpose, the depth sections of past earthquakes have been analyzed along several profiles transverse to the

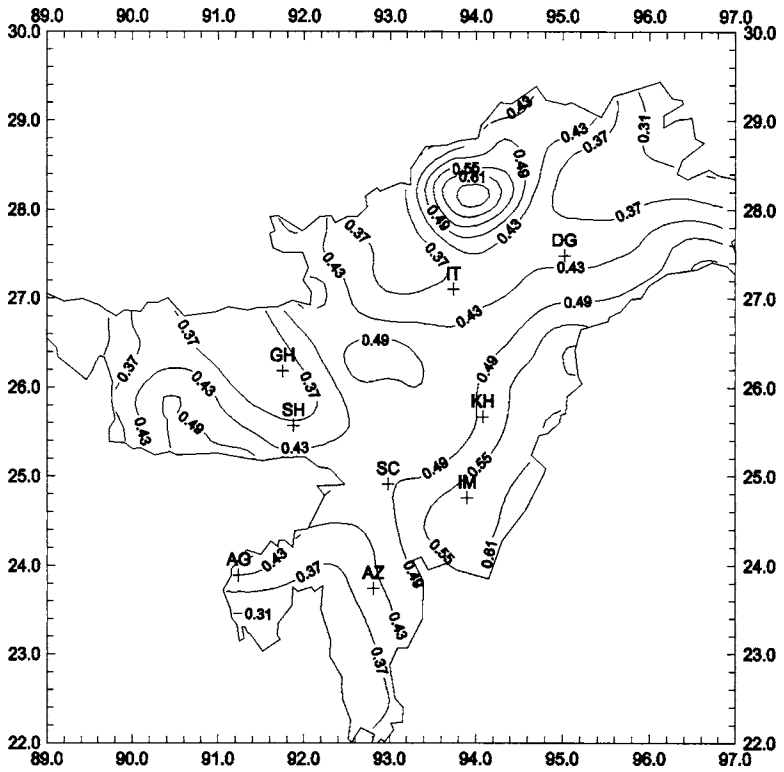

Figure 18. Hazard map for horizontal PSA (in g) at T=0.34 s.

major tectonic features in the region, and uniform average focal depths are assigned to the earthquakes in different areas of Northeast India as shown in Figure 11. The numbers, $n(M_j,R_i)$, are then subdivided into numbers for different average focal depths on the basis of the observed number of events for each value of the average focal depth.

Figure 12 shows the probability distribution of Equation 9, as computed for T =0.04, 0.50, and 1.0 s, in the case of the horizontal component for the (27.2° latitude, 93.7° longitude) grid point when the exposure period is 100 years. When $P[\mathrm{PSV}(T)]$ is known for several natural periods, a uniform hazard spectrum curve can be obtained for a given probability of exceedance, p, by drawing a horizontal line and by reading those PSV values at which this line intersects with the distribution curves for different values of T. Figure 13 shows the plots of the so-obtained (5% damping) UHS for PSA(T) for horizontal (v=0) motion, with p=0.5, at four different grid points defined by (26.0° latitude, 91.0° longitude; 28.0° latitude, 93.0° longitude; 25.0° latitude, 94.0° longitude; 29.0° latitude, 95.0° longitude). The corresponding results for vertical (v=1) motion are shown in Figure 14. From the results in Figures 13 and 14 it is seen that the UHS shapes vary significantly with the geographic coordinates, and thus to get more realistic design response spectra it is necessary to prepare several seismic zoning maps in terms of the

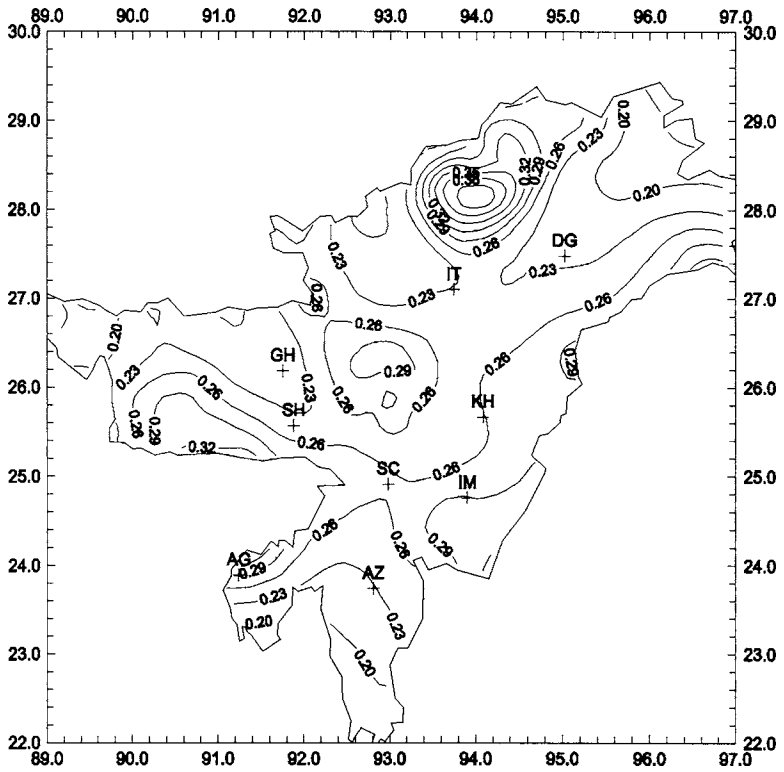

Figure 19. Hazard map for horizontal PSA (in g) at $T=0.7$ s.

spectral amplitudes at different natural periods (Lee and Trifunac 1987). By obtaining the UHS for all the grid points, seismic hazard maps can be obtained in terms of PSA (in g) contours. A total of six hazard maps for 5% damping PSA are shown in Figures 15–20, corresponding to $T=0.04$, 0.08, 0.17, 0.34, 0.70, and 1.0 s, respectively, for $p=0.50$, $Y=100$ years, and the horizontal component of ground motion.

From the hazard maps shown in Figures 14–19, a general pattern consistent with some of the geological characteristics of the region is quite obvious. The contours passing through Manipur and Mizoram are parallel to the folded belt of Tripura and western part of Arakan Yoma (see seismotectonic map of the Northeast India region in Figure 8). The Naga Thrusts, having a northeast-to-southwest strike, include several overthrust sheets. The contours in that area are parallel to that strike, and the values decrease as one goes away, thus indicating Naga Thrusts as one of the potential sources of seismicity. A high value of hazard level in the western part of Arunachal Pradesh reflects the fact that lots of earthquakes have taken place close to that region. In view of these observations, the objective model of seismicity adopted in this study appears to be acceptable for the Northeast India region, even though this is not based on any identification of the actual source zones of the region, which may be quite subjective.

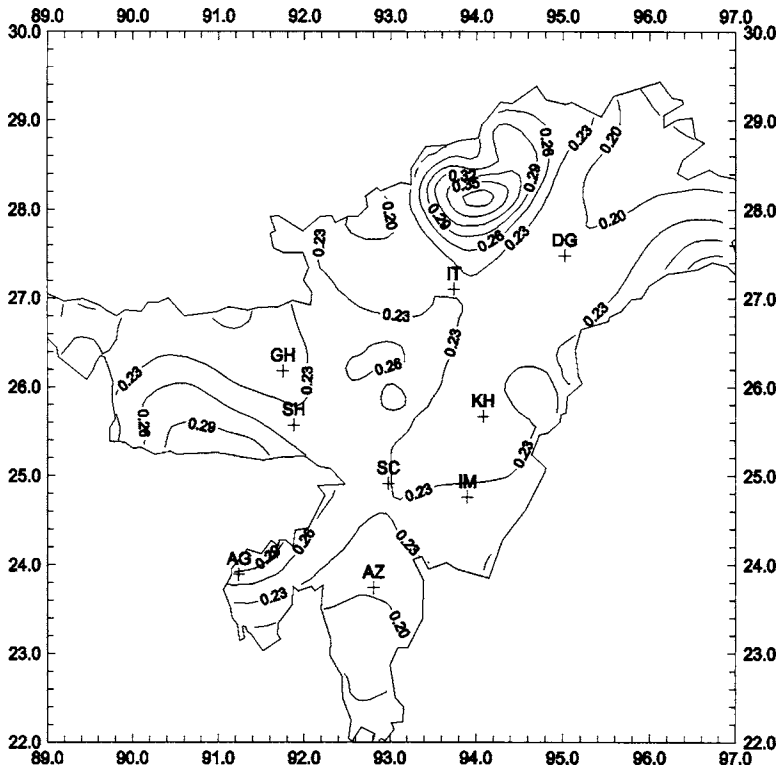

Figure 20. Hazard map for horizontal PSA (in g) at $T=1.0$ s.

It may be mentioned that the proposed hazard maps are specifically for the stiff sites (firm ground or sedimentary rock), due to the data used in the development of underlying attenuation model. Thus the information available from these maps may need further processing for use in case of medium to soft soil deposits at a site.

SUMMARY AND CONCLUSIONS

A probabilistic seismic hazard analysis based on the uniform hazard spectra for PSV has been carried out in Northeast India. For this purpose, a spectral attenuation model has been developed by using a total of 261 accelerograms recorded at different stations on stiff sites in the region. The proposed model is able to capture the frequency-dependent variations in PSV, and properly accounts for the effects of earthquake magnitude, epicentral distance, and focal depth on the PSV spectral shapes, for both horizontal and vertical motions. A regionalization-free approach has then been proposed to define the seismicity model of the region of interest. This approach is based on the data of past earthquake events over a long period of time from 1458 to 2000. In this approach, the entire region is divided into a fine grid of around 2,500 nodes, and hazard level is predicted for each of the nodes by assuming it to be dependent on the earthquake

events within a 300-km-radius area. The number of events expected to occur in different magnitude classes is obtained from the G-R relationship conforming to the data of past earthquake events. Using the spatial distribution of past earthquakes, these are then distributed among 50 source elements, with each source element assumed to be representing an annular-shaped area around the node of interest. Even though actual seismotectonic source zones are not identified in this approach, the estimated hazard mapping is found to be consistent with the main tectonic features in the northeast region.

Seismic hazard maps for 50% confidence level and ten natural periods between 0.04 and 1.0 s have been presented in terms of 5% damping PSA contours on stiff grounds. These maps provide much more detailed and direct information about the seismic hazard than those based on the use of PGA together with a standard spectral shape.

REFERENCES

Anderson, J. G., and Trifunac, M. D., 1977. *On Uniform Risk Functionals Which Describe Strong Earthquake Ground Motion: Definition, Numerical Estimation, and an Application to the Fourier Amplitude of Acceleration*, Report CE 77-02, University of Southern California, Los Angeles, CA.

Anderson, J. G., and Trifunac, M. D., 1978. Uniform risk functionals for characterization of strong earthquake ground motion, *Bull. Seismol. Soc. Am.* **68**, 205–218.

Bapat, A., Kulkarni, R. C., and Guha, S. K., 1983. *Catalogue of Earthquakes in India and Neighbourhood from Historical Period up to 1979*, Indian Society of Earthquake Technology, Roorkee, India.

Basu, S., and Nigam, N. C., 1978. On seismic zoning map of India, *Proceedings, VI Symposium on Earthquake Engineering*, Roorkee, India, Vol. I, pp. 83–90.

Bernreuter, D. L., Savy, J. B., Mensing, R. W., and Chen, J. C., 1989. Seismic Hazard Characterization of 69 Nuclear Power Plant Sites East of the Rocky Mountains, NUREG/CR-5250, U.S. Nuclear Regulatory Commission.

Bhatia, S. C., Ravikumar, M., and Gupta, H. K., 1999. A probabilistic seismic hazard map of India and adjoining regions, *Annali Di Geofisica* **42** (6), 1153–1164.

Chandrasekaran, A. R., and Das, J. D., 1993. *Strong Earthquake Ground Motion Data in EQINFOS for India: Part 1B*, Univ. of Roorkee and Univ. of Southern California, Dept. of Civil Eng., Report No. CE93-04, edited by M. D. Trifunac, M. I. Todorovska, and V. W. Lee.

Cornell, C. A., 1968. Engineering seismic risk analysis, *Bull. Seismol. Soc. Am.* **58**, 1583–1606.

Douglas, J., 2001. *A Comprehensive Worldwide Summary of Strong-Motion Attenuation Relationships for Peak Ground Acceleration and Spectral Ordinates* (*1969 to 2000*), ESEE Report No. 01-1, Imperial College of Science, Technology and Medicine, Civil Eng. Dept., London, U.K.

Douglas, J., 2002. Errata of and addition to ESEE Report No. 01-1.

Electric Power Research Institute (EPRI), 1986. *Seismic Hazard Methodology for the Central and Eastern United States*, Report NP-4726, Palo Alto, CA.

Frankel, A., 1995. Mapping seismic hazard in the central and eastern United States, *Seismol. Res. Lett.* **66** (4), 8–21.

Gupta, I. D., 2002. Should normalised spectral shapes be used for estimating site-specific design ground motion? *Proceedings, 12th Symposium on Earthquake Engineering*, Roorkee, Vol. I, pp. 168–175.

Gutenberg, B., and Richter, C. F., 1944. Frequency of earthquakes in California, *Bull. Seismol. Soc. Am.* **34**, 185–188.

Joyner, W. B., and Boore, D. M., 1981. Peak horizontal acceleration and velocity from strong motion records including records from the 1979 Imperial Valley, California, earthquake, *Bull. Seismol. Soc. Am.* **71** (6), 2011–2038.

Kaila, K. L., and Rao, N. M., 1979. Seismic zoning maps of Indian subcontinent, *Geophys. Res. Bull.* **17**, 293–301, National Geophysical Research Institute, Hyderabad, India.

Khattri, K. N., Rogers, A. M., and Algermissen, S. T., 1984. A seismic hazard map of India and adjacent areas, *Tectonophysics* **108**, 93–134.

Lee, V. W., 1992. On strong motion risk functionals computed from general probability distributions of earthquake recurrence, *Soil Dyn. Earthquake Eng.* **11**, 357–367.

Lee, V. W., 2002. Empirical scaling of strong earthquake ground motion—Part I: Attenuation and scaling of response spectra, *ISET J. Earthquake Technol.* **11** (4), 219–254.

Lee, V. W., and Trifunac, M. D., 1979. Automatic Digitization and Processing of Strong Motion Accelerograms, Report No. CE79-15 I and II, Univ. of Southern California, Dept. of Civil Eng., Los Angeles, CA.

Lee, V. W., and Trifunac, M. D., 1987. *Microzonation of a Metropolitan Area*, Report No. CE87-02, Univ. of Southern California, Dept. of Civil Eng., Los Angeles, CA.

McGarr, A., 1984. Scaling of ground motion parameters, state of stress, and focal depth, *J. Geophys. Res.* **89**, 6969–6979.

Orozova, I. M., and Suhadolc, P., 1999. A deterministic-probabilistic approach for seismic hazard assessment, *Tectonophysics* **312**, 191–202.

Peruzza, L., Slejko, D., and Bragato, P. L., 2000. The Umbria-Marche case: Some suggestions for the Italian seismic zonation, *Soil Dyn. Earthquake Eng.* **20**, 361–371.

Senior Seismic Hazard Analysis Committee (SSHAC), 1997. Recommendations for Probabilistic Seismic Hazard Analysis: Guidance on Uncertainty and Use of Experts, NUREG/CR-6372, U.S. Nuclear Regulatory Commission.

Stepp, J. C., 1973. *Analysis of completeness of the earthquake sample in the Puget Sound area*, in *Seismic Zoning*, edited by S. T. Harding, Report ERL 267-ESL30, NOAA Tech, Boulder, CO.

Todorovska, M. I., 1994. Comparison of response spectrum amplitudes from earthquakes with lognormally and exponentially distributed return period, *Soil Dyn. Earthquake Eng.* **13** (2), 97–116.

Todorovska, M. I., Gupta, I. D., Gupta, V. K., Lee, V. W., and Trifunac, M. D., 1995. *Selected Topics in Probabilistic Seismic Hazard Analysis*, Report No. CE95-08, Dept. of Civil Eng., Univ. of Southern California, Los Angeles, CA.

Trifunac, M. D., 1971. Zero base-line correction of strong-motion accelerograms, *Bull. Seismol. Soc. Am.* **61** (5), 1201–1211.

Trifunac, M. D., 1972. A note on correction of strong-motion accelerograms for instrument response, *Bull. Seismol. Soc. Am.* **62** (1), 401–409.

Trifunac, M. D., 1980. Effects of site geology on amplitudes of strong motion, *Proceedings, 7th World Conference on Earthquake Engineering*, Vol. 2, pp. 145–152.

Trifunac, M. D., 1990. A microzonation method based on uniform risk spectra, *Soil Dyn. Earthquake Eng.* **9** (1), 34–43.

Trifunac, M. D., 1992. Should peak acceleration be used to scale design spectrum amplitude? *Proceedings, 10th World Conference on Earthquake Engineering*, Madrid, Spain, Vol. 10, pp. 5817–5822.

Trifunac, M. D., and Lee, V. W., 1989. Empirical models for scaling pseudo relative velocity spectra of strong earthquake accelerations in terms of magnitude, distance, site intensity and recording site conditions, *Soil Dyn. Earthquake Eng.* **8** (3), 126–144.

Trifunac, M. D., and Lee, V. W., 1990. Frequency-dependent attenuation of strong earthquake ground motion, *Soil Dyn. Earthquake Eng.* **9** (1), 3–15.

Veneziano, D., Cornell, C. A., and O'Hara, T., 1984. *Historic Method for Seismic Hazard Analysis*, Report NP-3438, Electric Power Research Institute, Palo Alto, CA.

Verma, R. K., Mukhopadhyay, M., and Ahluwalia, M. S., 1976. Seismicity, gravity, and tectonics of Northeast India and Northern Burma, *Bull. Seismol. Soc. Am.* **66** (5), 1683–1694.

Wahlström, R., and Grünthal, G., 2001. Probabilistic seismic hazard assessment (horizontal PGA) for Fennoscandia using the logic tree approach for regionalization and nonregionalization models, *Seismol. Res. Lett.* **72** (1), 33–45.

Weichert, D. H., 1980. Estimation of earthquake recurrence parameters for unequal observational periods for different magnitudes, *Bull. Seismol. Soc. Am.* **70**, 1337–1346.

Wheeler, R. L., and Mueller, C. S., 2001. Central U.S. earthquake catalog for hazard maps of Memphis, Tennessee, *Eng. Geol.* **62**, 19–29.

Woo, G., 1996. Kernel estimation methods for seismic hazard area source modeling, *Bull. Seismol. Soc. Am.* **86**, 353–362.

(Received 25 April 2004; accepted 2 May 2005)